Journal of Sound and Vibration (2000) **231**(4), 989–1005
doi:10.1006/jsvi.1999.2319, available online at http://www.idealibrary.com on IDEAL®

DYNAMIC STABILITY OF A COMPLETELY FREE CIRCULAR CYLINDRICAL SHELL SUBJECTED TO A FOLLOWER FORCE

S.-H. Park and J.-H. Kim

Department of Aerospace Engineering, Seoul National University, San 56-1, *Shinrim-Dong, Kwanak-Ku, Seoul* 151-742, *Korea*

(*Received* 22 *September* 1998, *and in final form* 13 *January* 1999)

The dynamic stability of a completely free isotropic circular cylindrical shell under a follower force is investigated. First order shear deformation is included and the axial stress is assumed to be uniformly distributed through the thickness. A finite element model of the shell is formulated using a ring element in the circumferential direction and a Lagrangian element in the longitudinal direction. The dynamic stability is studied for various dimensionless lengths and thicknesses. The numerical results for the shells are compared with those of a beam model having equivalent dimensions. The analysis shows that the Rayleigh mode and the Love mode have an effect on instability and that the shell structure can be analyzed with a beam model within only a certain range of shell dimensions.

1. INTRODUCTION

A free–free beam model or a free-edged rectangular plate model has been used to study the dynamic stability of flexible aerospace structures and missiles. On the other hand, although the cylindrical shell is one of the basic elements commonly used in aerospace structures, the investigation of cylindrical shells under a follower force is as yet unavailable. As a matter of fact, the rocket or missiles, which have been researched using a beam model in many papers, are cylindrical shell structures rather than beams.

For studies of a free–free beam under follower forces, there are many papers in the literature. Beal [1] first investigated a free–free beam under a constant thrust and a pulsating thrust using the Euler–Bernoulli beam theory. He considered the effect of the control parameter and found two instability types, which were a flutter type and a divergence type. Wu [2] studied the relation between the critical load and the eigencurves using the finite element method. Park and Mote [3] investigated the effect of a concentrated mass on the critical load and the instability type. Park [4] treated a beam model with various rotary inertia and shear deformation parameters using element method.

0022-460X/00/140989 + 17 $35.00/0

Several papers on the dynamic stability of plates under a follower force are also available. A completely free plate subjected to a follower force was studied first by Higuchi and Dowell [5, 6]. They classified the plates into two categories which were beam-like plates and rectangular plates. In these papers, the effect of damping on stability was also researched. Kim and Park [7] treated the problem for various locations and magnitudes of intermediate follower forces using the finite element method.

Studies on the stability of cylindrical shells have been carried out only for the case of conservative loads. In addition, most of these works did not include the free–free edge condition. Matsunaga [8] studied the free vibration of a thick cylindrical shell subjected to axial stresses. He used a higher order shear deformation theory and treated a simply supported edge condition. There are many papers which treat the dynamic stability of cylindrical shells under a pulsating axial force [9–11], but in these papers, only a conservative load was treated and the movable edge conditions were not considered. There is work on the dynamic stability of a shell under non-conservative follower force [12]. In addition to free-edge condition, various boundary conditions were treated in that paper. However it deals with a shallow shell rather than a completely cylindrical shell.

In this work, the dynamic stability of completely free isotropic cylindrical shells under follower forces is studied using the finite element method. Shear deformation and rotary inertia are included in the potential energy and the kinetic energy. The unperturbed stress distribution is assumed to be uniform through the thickness and to be linear along the longitudinal direction. Due to the fact that the rigid-body mode cannot be reproduced by using the Lagrangian element in the shell co-ordinate, the trigonometric ring element in the circumferential direction and the 4-node Lagrangian element in the longitudinal direction are used. A free–free shell has Rayleigh modes and Love modes as the two lowest modes when the number of circumferential waves is equal to or greater than two [13]. Since the critical load is related to the lowest eigenvalues, the Rayleigh mode and the Love mode may have an effect on the stability of the free–free shells. The critical loads are calculated for various lengths and thicknesses. A beam model equivalent to the shell dimensions' is analyzed and compared with the results of a shell-model analysis.

2. FORMULATION

Figure 1 shows a cylindrical shell of length L, thickness h and radius R. The x-axis is taken along a generator, the circumferential arc length subtends an angle θ, and the z-axis is directed radially outwards. A follower force with the magnitude P is assumed to be uniformly distributed along an edge at $x = 0$ and to be tangential to the deformed generator (Figure 2).

Now, if we include only first- order shear deformation, the displacement field can be written as [14]

$$\begin{aligned} u &= u_0(x, \theta) + z\phi(x, \theta), \\ v &= v_0(x, \theta) + z\psi(x,.\theta), \\ w &= w_0(x, \theta), \end{aligned} \tag{1}$$

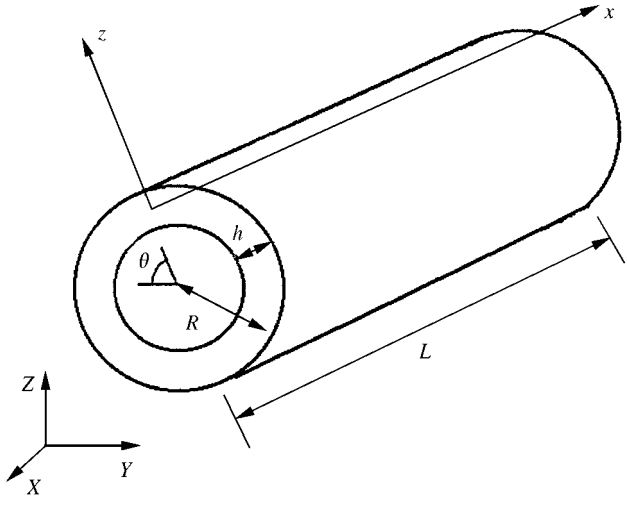

Figure 1. Co-ordinate system of a circular cylindrical shell.

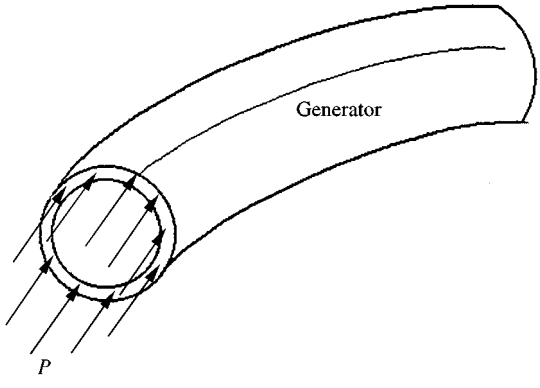

Figure 2. Follower force in deformed geometry.

where u_0, v_0 and w_0 are the displacements of the middle surface, and ϕ and ψ are the changes of slope of the normal to the middle surface. In thin-shell theories ϕ and ψ are functions of w_0 and v_0. But, ϕ and ψ should be independent of order variables to take the shear deformation effect into account. Using equation (1), we get the kinetic energy as

$$T = \frac{1}{2}\rho \int_0^{2\pi} \int_0^{L} \int_{-h/2}^{h/2} (\dot{u}_0^2 + \dot{v}_0^2 + \dot{w}_0^2 + 2z\dot{u}_0\phi + 2z\,\dot{v}_0\dot{\psi} + z^2\dot{\phi}^2 + z^2\dot{\psi})$$

$$\times (R + z)\,\mathrm{d}z\,\mathrm{d}x\,\mathrm{d}\theta, \tag{2}$$

where ρ is the mass density of the shell material. The strain energy is written as

$$V = \frac{1}{2}\int_0^{2\pi}\int_0^{L}\int_{-h/2}^{h/2} \varepsilon^{\mathrm{T}}\mathbf{Q}\varepsilon(R+z)\,\mathrm{d}z\,\mathrm{d}x\,\mathrm{d}\theta, \tag{3}$$

where

$$\varepsilon = \begin{bmatrix} \varepsilon_{xx} \\ \varepsilon_{\theta\theta} \\ \gamma_{x\theta} \\ \gamma_{xz} \\ \gamma_{\theta z} \end{bmatrix} = \begin{bmatrix} \dfrac{\partial u_0}{\partial x} + z\dfrac{\partial \phi}{\partial x} \\ \dfrac{1}{R+z}\left(\dfrac{\partial v_0}{\partial \theta} + w_0\right) + \dfrac{z}{R+z}\dfrac{\partial \phi}{\partial \theta} \\ \dfrac{\partial v_0}{\partial x} + z\dfrac{\partial \psi}{\partial x} + \dfrac{1}{R+z}\dfrac{\partial u_0}{\partial \theta} + \dfrac{z}{R+z}\dfrac{\partial \phi}{\partial \theta} \\ \phi + \dfrac{\partial w_0}{\partial x} \\ \psi + \dfrac{1}{R+z}\left(\dfrac{\partial w_0}{\partial \theta} - v_0\right) - \dfrac{z}{R+z}\psi \end{bmatrix}, \tag{4}$$

$$\boldsymbol{\sigma} = \mathbf{Q}\varepsilon, \tag{5}$$

$$\boldsymbol{\sigma} = \begin{bmatrix} \sigma_{xx} \\ \sigma_{\theta\theta} \\ \sigma_{x\theta} \\ \sigma_{xz} \\ \sigma_{\theta z} \end{bmatrix}, \tag{6}$$

The shear correction factor and the material properties are included in the matrix $\boldsymbol{\sigma}$. In equation (4), we refer to reference [14].

An extended Hamilton's principle is applied to a shell subjected to a tangential follower force as follows:

$$\int_{t_1}^{t_2} (\delta T - \delta U + \delta W_f)\,\mathrm{d}t = 0, \tag{7}$$

where δW_f is the virtual work of the follower force. Taking the acceleration of the shell by the follower force into account, we can assume that the axial stress is linearly distributed along the longitudinal direction [15]. In addition, assuming that the axial stress is uniformly distributed in the thickness direction, δW_j is expressed as

$$\delta W_f = \int_0^{2\pi}\int_0^{L} \frac{P}{L}(L-x)\left(\frac{\partial \delta w_0}{\partial x}\frac{\partial w_0}{\partial x} + \frac{\partial \delta v_0}{\partial x}\frac{\partial v_0}{\partial x}\right) R\,\mathrm{d}x\,\mathrm{d}\theta$$

$$+ \int_0^{2\pi} P\left(\delta w_0 \frac{\partial w_0}{\partial x} + \delta v_0 \frac{\partial v_0}{\partial x}\right) R\,\mathrm{d}\theta|_{x=0}, \tag{8}$$

where P is the constant magnitude of a follower force per unit length. In the expression of δW_f, the work induced by v is excluded generally for plates [5], but, in equation (8), the circumferential displacement v is included due to the fact that the vibration of shells induces much displacement in the circumferential direction as compared with the plate vibration. In addition, the torsional effect on stability can be included by considering the term containing v. Though v is composed of v_0 and $z\psi$, the term involving ψ is about in equation (8), due to the fact that $z\psi$ is small enough to be neglected in comparision with v_0.

To solve the variational form, equation (7), we introduce the circumferential base functions as [14]

$$u_0 = \sum_{m=0}^{\infty} U(x)\cos(m\theta)e^{i\omega t},$$

$$v_0 = \sum_{m=0}^{\infty} V(x)\sin(m\theta)e^{i\omega t},$$

$$w_0 = \sum_{m=0}^{\infty} W(x)\cos(m\theta)e^{i\omega t},$$

$$\phi = \sum_{m=0}^{\infty} \Phi(x)\cos(m\theta)e^{i\omega t},$$

$$\psi = \sum_{m=0}^{\infty} \Psi(x)\sin(m\theta)e^{i\omega t},$$

$$m = 0, 1, 2, \ldots, \tag{9}$$

With the above shape functions for the circumferential direction, the 4-node Lagrangian element can be used for the longitudinal direction. The shape functions in equations (6) are identical with the mode shapes of the circumferential direction for the isotropic case.

Now, examining equation (8), we can infer that δW_f has the orthogonal property about the circumferential base functions (9). With different m's. In other words, the modes with different circumferential wave numbers can be decoupled. Using this property, the stability analysis can be performed for each circumferential wave number respectively. As regards efficiency, one can save much time by virtue of the smaller matrix size.

Using the finite element method with the above base functions, we obtain eigenvalue equations as follows:

$$det[-\omega^2\mathbf{M}^{(m)} + \mathbf{K}^{(m)} + P\mathbf{S}^{(m)}] = 0, \quad m = 0, 1, 2, 3, \ldots. \tag{10}$$

The superscript m indicates the circumferential wave number.

By introducing non-dimensional parameters such as x/R, z/R, L/R and h/R, the following parameters are induced:

$$\beta = P\frac{(1-v^2)}{Eh}, \tag{11}$$

$$\lambda^2 = \omega^2\frac{(1-v^2)\rho R^2}{E}. \tag{12}$$

Then, equations (10) can be written as

$$det[-\lambda^2 \mathbf{M}^{(m)} + \mathbf{K}^{(m)} + \beta \mathbf{S}^{(m)}] = 0, \tag{13}$$

where **M**, **K** and **S** are non-dimensional matrices.

The stability of the cylindrical shell can be examined by checking the sign and the imaginary part of λ^2. The coalescence of two eigenvalues of equation (13) indicates a flutter type instability and eigenvalues become complex numbers. If an eigenvalue of equation (13) reduces to zero, a divergence type instability occurs.

3. EQUIVALENT BEAM

For a Timoshenko beam model, the non-dimensional parameters are the shear deformation parameter $\kappa GAL^2/EI$ and the rotary inertia parameter I/AL^2, where κGA is the shear stiffness and EI is the bending rigidity. In constructing the equivalent beam model, the material properties must be identical to the considered shell properties, and the shear correction factor κ can be determined by the shape of the shell cross section as [16]

$$\kappa = \frac{6(1+\nu)(1+k)^2}{(7+6\nu)(1+k)^2 + (20+12\nu)k^2}, \tag{14}$$

where

$$k = \frac{R - h/2}{R + h/2}.$$

For a circular cross-section, A and I can be written as

$$A = 2\pi Rh, \tag{15}$$

$$I = \pi R^3 h, \tag{16}$$

where R and h are the radius and the thickness of the shell respectively. Then assuming that the lengths of the shell and the beam are the same, I/AL^2 can be determined as

$$\frac{I}{AL^2} = \frac{R^2}{2L^2}. \tag{17}$$

Considering that the follower force of the beam is assumed to be a concentrated load and that P in Figure 2 is a distributed load, the equivalent non-dimensional follower force can be written by means of the non-dimensional follower force of the beam as

$$\beta_{eq} = \beta_b \frac{(1-\nu)^2}{2} \frac{R^2}{L^2}, \tag{18}$$

where β_b is the non-dimensional follower force of the beam. Using these parameters, the results of a beam model can be compared with those of a shell model.

4. NUMERICAL RESULTS

The ratio z/R was not neglected in the integration of strain energy and kinetic energy expressions involving $(1 + z/R)$. The number of elements in the longitudinal direction is based on the convergence of natural frequency. Figure 3 shows the convergence of non-dimensional natural frequencies. The analytic solution of these cases is 4.00E-6 in reference [13], in which the solution is based on Flügge's shell theory. In Figure 3, use of 10 elements can reduce the computational error below 1% in both cases. Therefore, in computing the critical load, 20 elements for the longitudinal direction were used and enough to get accurate results.

Eight circumferential wave numbers $(0, 1, 2, \ldots, 7)$ were considered for the stability check and the lowest critical loads were found below $m = 7$ for the considered shell dimensions. The shear correction factor and Poisson's ratio were assumed to be $\pi^2/12$ and 0·3 respectively.

The critical forces for the beam model were obtained using the finite element method and compared with those of Reference [4]. They agreed well with each other, and so only the computed results will be shown in the figures.

On the basis of the numerical results showing two clearly different tendencies, the cylindrical shells of the considered dimensions could be classified into two kinds, which are long and short shells.

4.1. LONG SHELL (L/R ⩾ 20)

Firstly, we must define and examine the mode shapes which induce various types of instability. The modes of a free–free cylindrical shell can be grouped by the

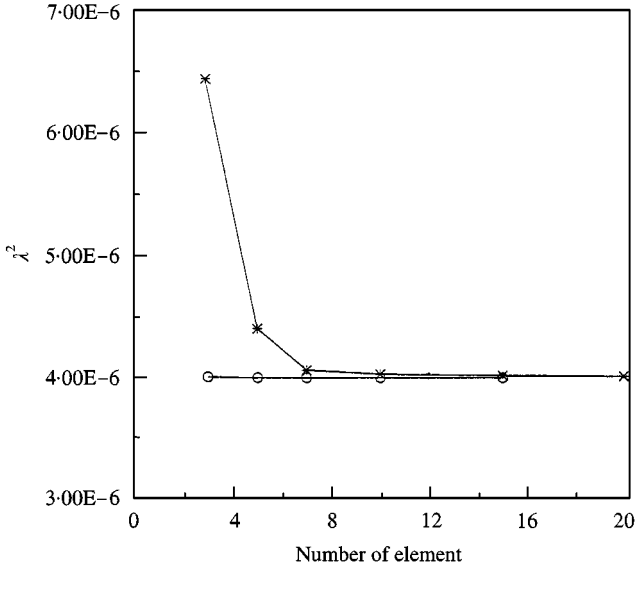

Figure 3. Convergence of non-dimensional natural frequency ($h/R = 0{\cdot}002$, m = 2). Mode number in longitudinal direction & L/R, ⊖ modeNo.: 1. $L/R = 61{\cdot}5$; —✳— mode No.: 5. $L/R = 224$.

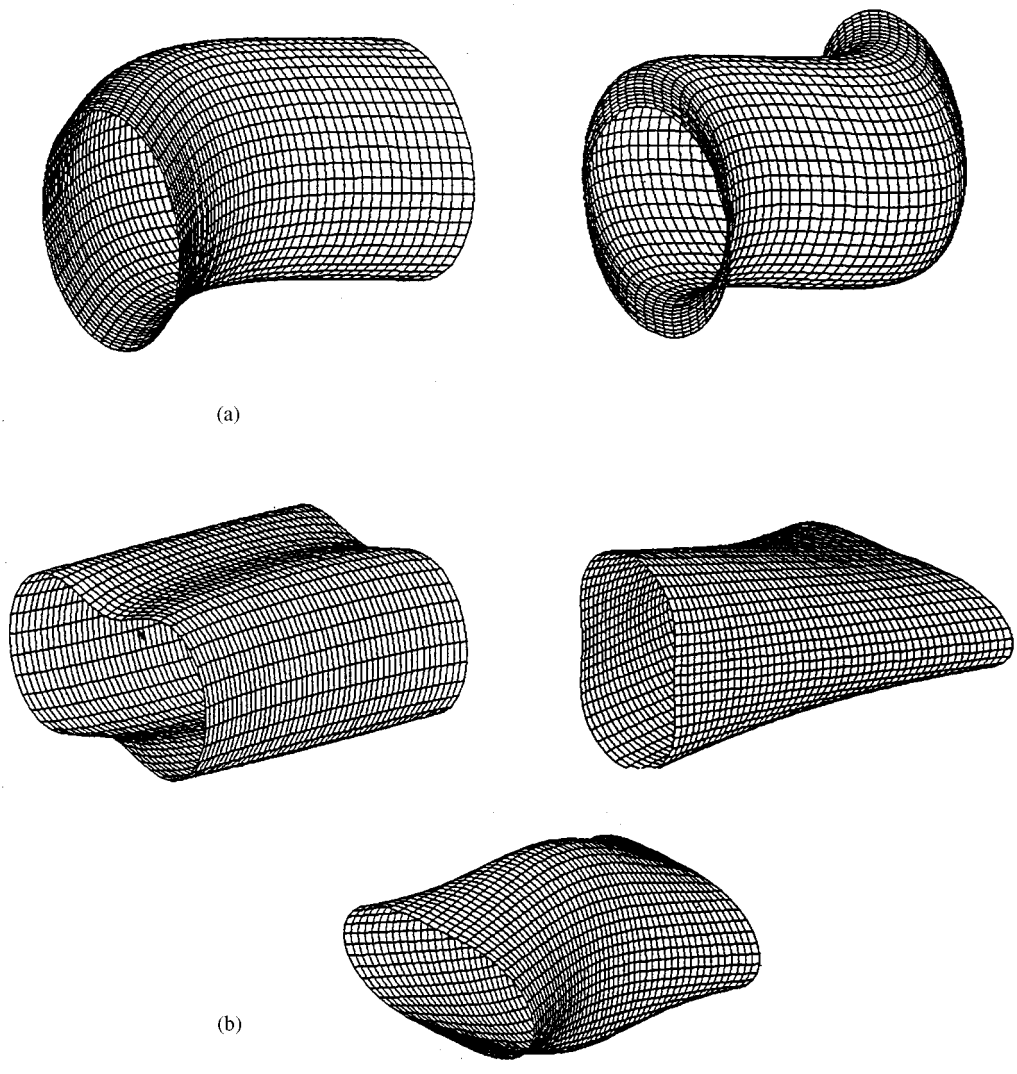

Figure 4. Shapes of various modes. (a) First bending and second bending modes ($m = 1$). (b) Rayleigh, Love and first bending modes ($m = 2$).

number of circumferential waves m. The case $m = 0$ is not examined, because the modes with $m = 0$ do not induce critical load. The mode shapes for $m = 1$ are beam-like modes as presented in Figure 4(a). In this work, those modes are called first bending mode, second bending mode and so forth by the number of extrema in the longitudinal direction. If the number of circumferential waves m is equal to or greater than two, the free–free cylindrical shell has two sets of modes which have a linear or constant axial deformation. The first set, analyzed by Rayleigh, does not vary axially, and the second set, analyzed by Love, has a linear variation (reference [13]). But, the exact mode shapes have a small curvature in the longitudinal direction as shown in Figure 4(b). Except for the two modes, the other modes have

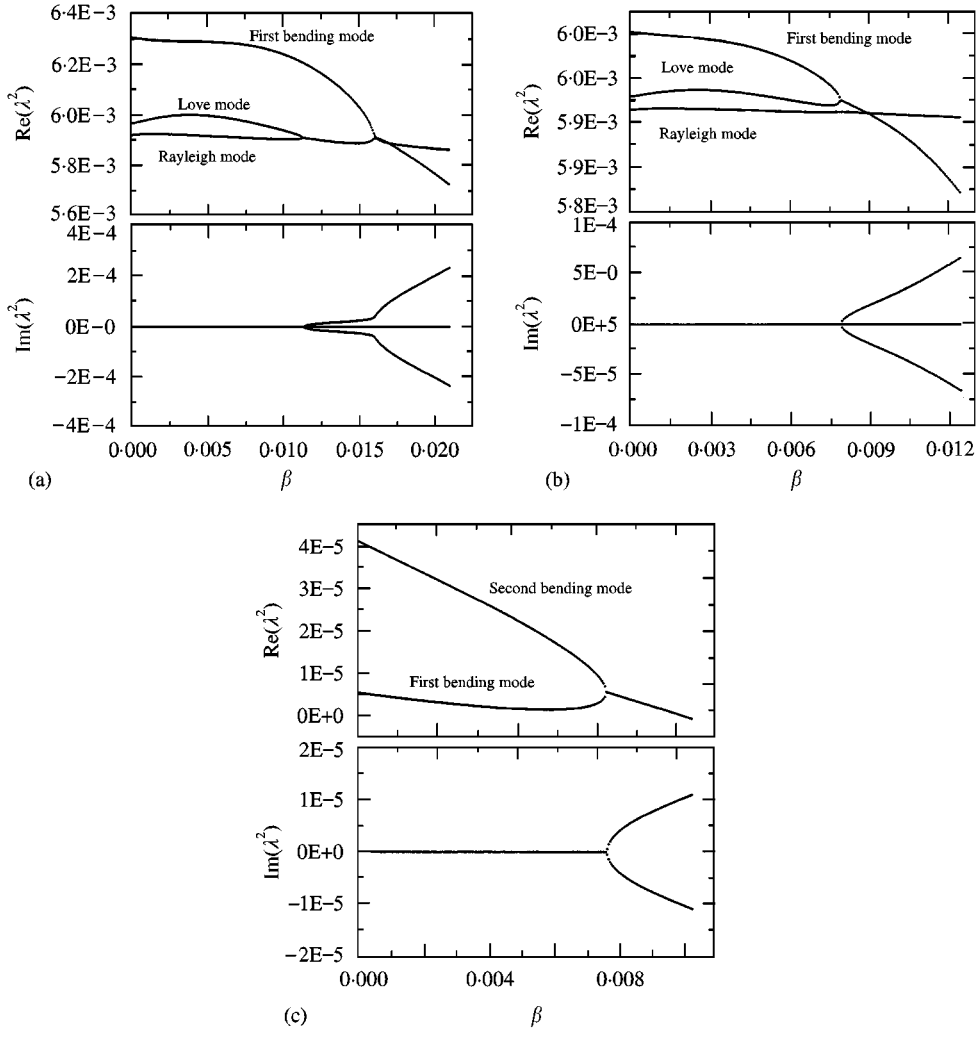

Figure 5. Eigenvalue curves for typical instability types. (a) $L/R = 20$, $h/R = 0{\cdot}1$, $m = 2$. (b) $L/R = 40$, $h/R = 0{\cdot}1$, $m = 2$. (c) $L/R = 80$, $h/R = 0{\cdot}13$, $m = 1$.

much bending in the longitudinal direction and are called the first bending mode, second bending mode and so on like the modes of $m = 1$.

Figure 5 shows the typical instability types of free–free cylindrical shells under a follower force. In most cases, these kinds of flutter instability determine the critical load. Although the divergence instability exists, the flutter instability occurs under a lower follower force. Figures 5(a) and (b) demonstrate that the Love mode and the Rayleigh mode play an important role in the stability of shells. If the circumferential wave number is equal to or higher than two, those types of instability take place. Due to the fact that the modes with $m = 1$ are beam-like modes, a beam-like instability can occur in shells as shown in Figure 5(c).

In Figures 5(a) and (b), the tendencies of eigenvalue curves are similar to each other, but the two modes including a flutter instability are the Love mode and the first bending mode in Figure 5(a) are the Rayleigh mode and the Love mode in Figure 5(b). Examining the imaginary parts of eigenvalues in Figure 5(b), one can see that the coalescence of the Rayleigh mode and the Love mode induce a temporary weak flutter from the fact that the imaginary parts of the complex eigenvalues remain small until the first bending mode eigenvalue approaches.

Table 1 shows the circumferential wave numbers in which an instability can be found under the lowest follower force among all the circumferential wave numbers. We can infer that the circumferential wave number decreases as the thickness and the length of a shell increase. The coalescence of the Rayleigh mode and the Love mode does not occur in the case of very long shell. In addition, the circumferential wave number showing the first instability reduces only to one.

Figure 6 shows the critical values versus thickness ratio for various lengths of shells. It can be seen that the critical load increases as the thickness ratio increases. There are several points on each line where the slope decreases as the thickness ratio increases. At these points, the circumferential wave number reduces to a lower

TABLE 1

Instabililty type and circumferential wave number determining the critical load

	$L/R = 20$		$L/R = 40$		$L/R = 60$		$L/R = 80$		$L/R = 100$	
h/R	m	Class	m	Class	m	Class	m	Class	m	Class
0·01	5	L + 1st	4	L + 1st	3	L + 1st	3	L + 1st	3	L + 1st
0·02	4	R + L	3	L + 1st	3	L + 1st	3	L + 1st	2	L + 1st
0·03	3	R + L	3	L + 1st	2	L + 1st	2	L + 1st	2	L + 1st
0·04	3	R + L	3	L + 1st	2	L + 1st	2	L + 1st	2	L + 1st
0·05	2	R + L	2	L + 1st	2	L + 1st	2	L + 1st	2	L + 1st
0·06	2	R + L	2	L + 1st	2	L + 1st	2	L + 1st	2	L + 1st
0·07	2	R + L	2	L + 1st	2	L + 1st	2	L + 1st	2	L + 1st
0·08	2	R + L	2	L + 1st	2	L + 1st	2	L + 1st	2	L + 1st
0·09	2	R + L	2	L + 1st	2	L + 1st	2	L + 1st	2	L + 1st
0·1	2	R + L	2	L + 1st	2	L + 1st	2	L + 1st	2	L + 1st
0·11	2	R + L	2	L + 1st	2	L + 1st	2	L + 1st	1	1st + 2nd
0·12	2	R + L	2	L + 1st	2	L + 1st	2	L + 1st	1	1st + 2nd
0·13	2	R + L	2	L + 1st	2	L + 1st	1	1st + 2nd	1	1st + 2nd
0·14	2	R + L	2	L + 1st	2	L + 1st	1	1st + 2nd	1	1st + 2nd
0·15	2	R + L	2	L + 1st	2	L + 1st	1	1st + 2nd	1	1st + 2nd
0·16	2	R + L	2	L + 1st	2	L + 1st	1	1st + 2nd	1	1st + 2nd
0·17	2	L + 1st	2	L + 1st	1	1st + 2nd	1	1st + 2nd	1	1st + 2nd
0·18	2	L + 1st	2	L + 1st	1	1st + 2nd	1	1st + 2nd	1	1st + 2nd
0·19	2	L + 1st	2	L + 1st	1	1st + 2nd	1	1st + 2nd	1	1st + 2nd
0·2	2	L + 1st	2	L + 1st	1	1st + 2nd	1	1st + 2nd	1	1st + 2nd

R + L: Coalescence of Rayleigh mode and Love mode.
L + 1st: Coalescence of Love mode and first bending mode.
1st + 2nd: Coalescence of first bending mode and second bending mode.

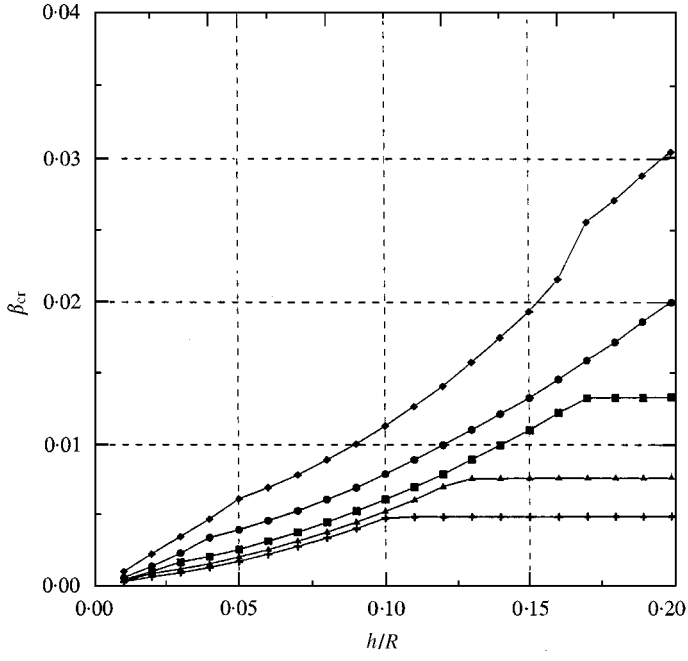

Figure 6. Critical load for various lengths of the shell. L/R: —◆— 20; —●— 40; —■— 60; —▲— 80; —+— 100.

value as listed in Table 1 or the flutter type changes to another one among the instability types in Figure 4. One can see that there exist some ranges along the horizontal axis where the critical load does not change with the increase of thickness ratio. These ranges are located in the region of large thickness ratios and enlarge as the length of the shell increases. Comparing the results of Table 1, it is seen that the flutter instability in Figure 5(c) occurs and the circumferential wave number of the modes inducing instability is one in that range. In other words, the shell behaves like a beam under a follower force in those ranges. Examining equations (14), (17) and (18), one can see that the critical load of an equivalent beam model depends on the thickness ratio only by the shear correction factor κ. For the range of thickness ratio considered in this work, κ, has an almost constant value (0.53–0.57) and therefore the thickness ratio of the shell has little effect on the critical load of the equivalent beam. Therefore, it is probable that the critical load in those ranges does not vary as the thickness ratio increases. But, the fact that the critical load is invariable in those ranges does not mean that the dimensional critical load remains constant though the thickness of the shell increases. For equation (11), we can infer that the dimensional critical load increases linearly in those ranges, as the thickness of the shell increases with the other dimensions of the shell constant.

Figures 7(a) and (b) show eigenvalue curves of the various thickness ratios. In case of $m = 2$, as the thickness ratio increases, the eigenvalue curves move considerably in the vertical direction, with the increase of the critical load

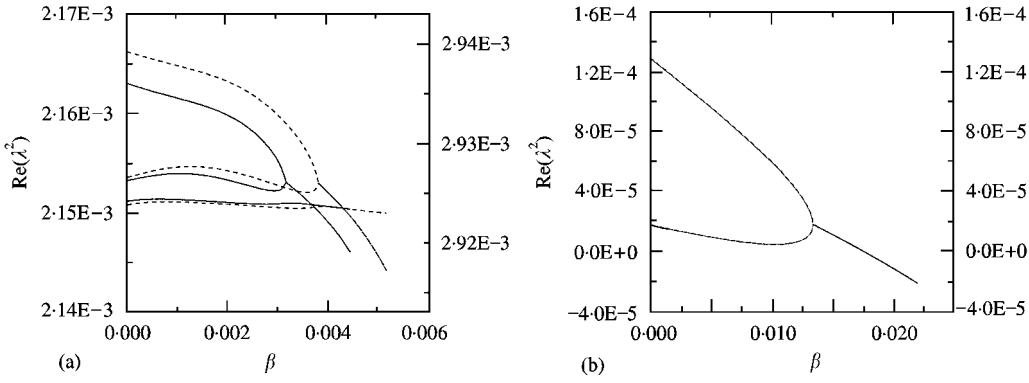

Figure 7. Eigenvalue curves for various thickness ratios. (a) $L/R = 60$, $m = 2$. h/R: —— 0·06 (left vertical axis); - - - - 0·07 (right vertical axis); (b)$L/R = 60$, $m = 1$. h/R: —— 0·19 (left vertical axis); - - - - 0·20 (right vertical axis).

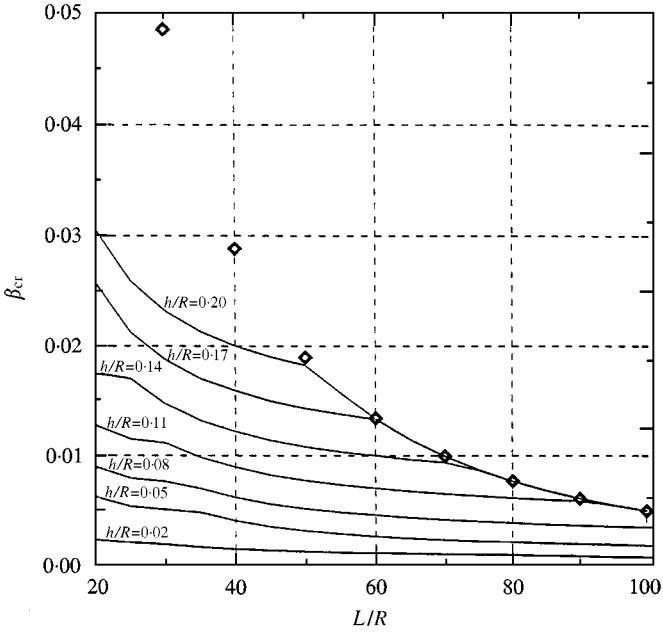

Figure 8. Critical load of shell and equivalent beam. —— shell; ♦ beam.

(Figure 7(a)). In Figure 7(b), two sets of the curves are almost identical and show the same critical load. These phenomena correspond to the above statements about Figure 6.

In Figure 8, we can compare the results of the equivalent beam model with the criticle load of the beam-like flutter ($m = 1$). From the explanation about χ in the above paragraph, the shear correction factor can be assumed to be constant while computing the critical load of the beam model. The critical loads for various

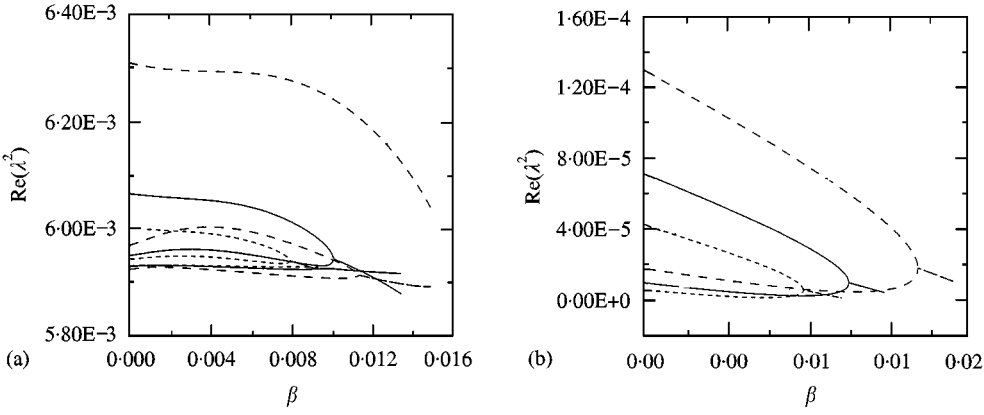

Figure 9. Eigenvalue curves for various length ratios. (a) $h/R = 0{\cdot}1$, $m = 2$. L/R: ---- 40; —— 30; – – 20. (b) $h/R = 0{\cdot}2$, $m = 1$. L/R: ---- 60; —— 70; – – 60.

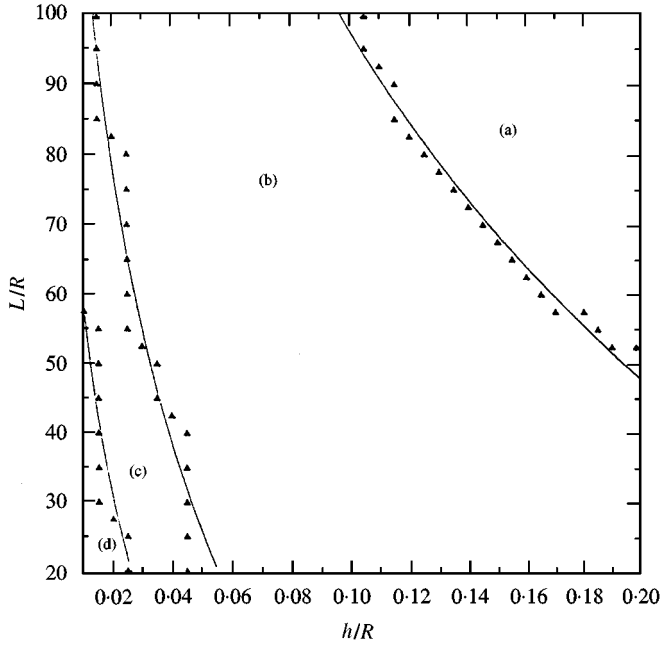

Figure 10. Region for each circumferential wave number determining critical load. ▲ sampled data points; —— fitted boundary. (a) $m = 1$ (beam-like flutter) (b) $m = 2$, (c) $m = 3$, (d) $m = 4$ or higher.

thickness ratios merge as the length of the shell increases. The merging of the critical loads is due to the fact that there exist some ranges where the critical load does not change even though the thickness ratio increases in Figure 6. It can be seen that the merged critical loads of shell coincide well with those of the equivalent beams in Figure 8. This means that a shell under a follower force might be analyzed by a beam model in the ranges of thickness and length where the beam-like modes induce the flutter instability.

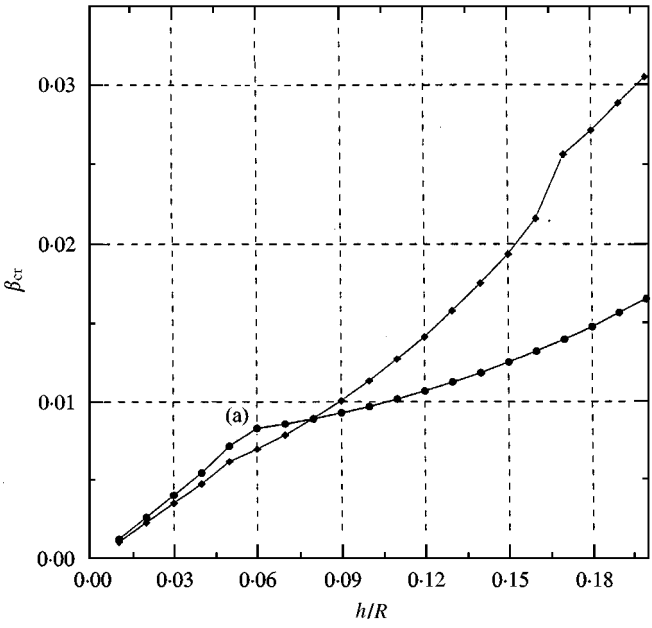

Figure 11. Critical load of short shells. L/R: —●— 15; —◆— 20.

The eigenvalue curves of various length ratios are presented in Figure 9. As the length ratio decreases, the critical loads increase without much translation of the eigencurves in the vertical direction. In Figure 9(a), one can see that the eigenvalues of the first bending mode increase most rapidly as the length ratio decreases. With this procedure, the difference between the eigencurves of the Rayleigh and Love modes become much smaller than that of the Love and first bending modes, and the coalescence of the Rayleigh and Love modes takes place as listed in Table 1.

Figure 10 shows the boundaries where the circumferential mode number determining the critical load changes. Only the shell belonging to region (a) can be analyzed using a beam model. One can see that the second circumferential modes are the critical modes in a wide range of thickness and length.

4.2. SHORT SHELL ($L/R < 20$)

For short shells, there exist instability types different from those of Figure 5. In Figure 11, it can be seen that the critical load of the shorter shell is lower than that of the longer shell for some range of thickness ratio. In the case of $L/R = 15$, the instability types presented in Figure 5 occur for the thin shells. But an instability of a different type takes place above the thickness ratio of the point (a), where the higher modes of $m = 1$ become unstable. Figure 12 shows that the ninth mode and the tenth mode having almost the same free-vibration eigenvalues become unstable.

Now, we must investigate the possibility of this type of instability in practical structures. One of the two modes having almost the same eigenvalues is the shear

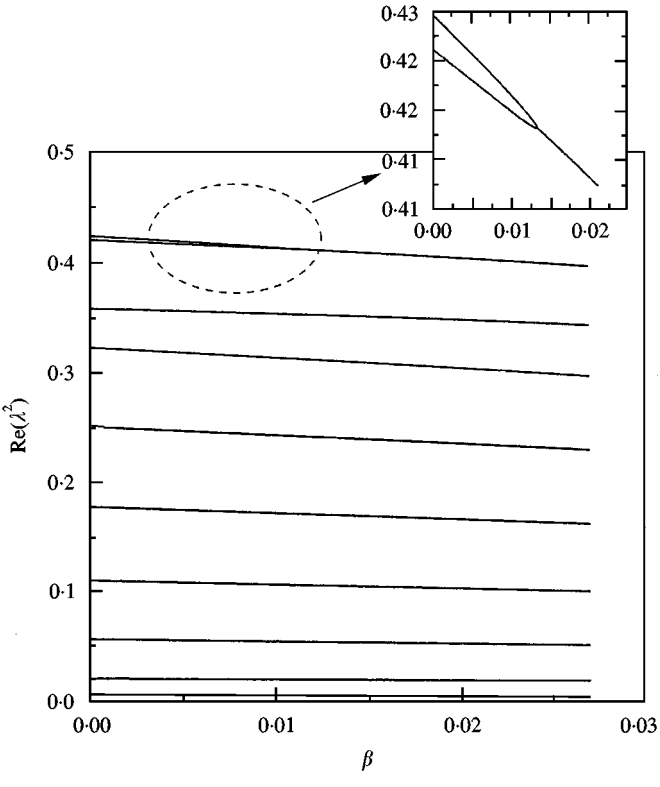

Figure 12. Eigenvalue curve for short shell ($L/R = 15$, $h/R = 0{\cdot}12$, $m = 1$).

mode as explained for a Timoshenko beam theory in reference [17]. In other words, those two modes have the same circumferential and axial wave number. If we examine the mode shapes of the ninth and the tenth modes in Figure 12, we may see that one of the modes has much transverse shear deformation. Due to the fact that the first order shear deformation theory can neither estimate the eigenvalues nor the mode shapes of the higher modes possessing much shear deformation, we cannot be sure that the higher mode instability occurs.

5. CONCLUDING REMARKS

A competely free circular cylindrical shell subjected to a follower force was investigated using a finite element method. The cylindrical shell can be analyzed by a beam model only in the case of thick and long shells. In these cases, the unstable modes are the first and second bending modes for which the circumferential wave number is one. These modes are similar to those of beams and the critical loads agree well with the results of the beam model. If the thickness and the length of the shells decrease, the critical conditions occur in the Rayleigh mode, the Love mode and the first bending mode for which the circumferential wave numbers are higher than one. In this case, a beam model cannot be applied to the shells. This means

that missile or rocket structures should be analyzed by a more exact model like shells rather than a beam model because the circumferential wave number of the unstable modes is not always one.

The results for short shells ($L/R < 20$) pose a problem in the dynamic stability analysis of shells. Due to the fact that the higher modes become unstable, the mode shapes and the eigenvalues of the unstable modes may have much numerical error. Therefore, the critical load is not exact, either. In addition to this problem , other problems are present in shell modelling for missile or rocket structures. Because the practical shell structures for missiles or rockets may have many stiffening elements, the Rayleigh mode or the Love mode may be absent. If so, the instability type may be altered into another one and the critical load may change very much. However, if the structure has an axisymmetric property like a cylindrical shell, the stability analysis can be performed by manipulations of the small matrix as was done in this paper using orthogonality.

ACKNOWLEDGMENT

This work was supported by the Korean Ministry of Education (Mechanical Engineering; ME 97-G-03).

REFERENCES

1. T. R. Beal 1995 *AIAA Journal* **30**, 486–494. Dynamic stability of a flexible missile under constant and pulsating thrust.
2. J. J. Wu *Journal of Sound and Vibration* **49**, 105–114. On the missile stability
3. Y. P. Park and C. D. Mote 1985 *Journal of Sound and Vibration* **98**, 247–256. The maximum controlled follower force on a free–free beam carrying a concentrated mass.
4. Y. P. Park 1987 *Journal of Sound and Vibration* **113**, 407–415. Dynamic stability of a free Timoshenko beam under a controlled follower force.
5. K. Higuchi and E. H. Dowell 1990 *AIAA Journal* **28**, 1300–1305. Dynamic stability of a rectangular plate with four free edges subjected to a follower force.
6. K. Higuchi and E. H. Dowell 1992 *AIAA Journal* **30**, 820–825. Effect of structural damping on flutter of plates with a follower force.
7. J. H. Kim and J. H. Park 1998 *Journal of Sound and Vibration*, **209**, 882–888. On the dynamic stability of rectangular plates subjected to intermediate follower forces.
8. H. Matsunaga 1998 *Journal of Sound and Vibration* **211**, 1–17. Free vibration of thick circular cylindrical shells subjected to axial stresses.
9. A. Vijayaraghavan and R. M. Evan-Iwanowski 1967 *Journal of Applied Mechanics* **34**, 985–990. Parametric instability of circular cylindrical shells.
10. K. Nagai and N. Yamaki 1978 *Journal of Sound and Vibration* **58**, 425–441. Dynamic stability of circular cylindrical shells under periodic compressive forces.
11. K. Y. Lam and T. Y. Ng 1997 *Journal of Sound and Vibration* **207**, 297–520. Dynamic stability of cylindrical shells subjected to conservative periodic axial loads using different shell theories.
12. M. N. Bismark-Nasr 1995 *AIAA Journal* **33**, 355–360. Dynamic stability of shallow shells subjected to follower forces.
13. R. D. Blevins 1979 *Formulas for Natural Frequency and Mode Shape*. New York: Litton Educational Publishing.
14. W. Soedel 1993 *Vibrations of Shells and Plates*. New York: Marcel Dekker.

15. MEIROVITCH 1967 *Analytical Methods in Vibrations*. New York: The Macmillan Company.
16. I. H. SHAMES and C. L. DYM 1973 *Solid Mechanics*. Tokyo: MeGraw-Hill Kogakusha, LTD
17. E. B. MAGRAB 1979 *Vibrations of Elastic Structural Members*. Alphen aan den Rijn, The Netherlands: Sijthoff & Noordhoff.
18. A. E. H. LOVE 1994 A *Treatise on the Mathematical Theory of Elasticity*. New York: Dover Publications.
19. L. H. DONNELL 1976 *Beams, Plates and Shells*. New York: McGraw-Hill Book Company.